Numerically enhancing daytime radiative cooling performance of random dielectric microsphere coatings by hollow structures

Meijie Chen[a],* Shuang Li,[a] Dan Pang,[a] Yanwei Zhao,[a] Yuan Yang,[b],* and Hongjie Yan[a],*

[a]Central South University, School of Energy Science and Engineering, Changsha, China
[b]Columbia University, Department of Applied Physics and Applied Mathematics, New York, United States

Abstract. Dielectric microsphere coatings for passive daytime radiative cooling (PDRC) are gaining attention owing to their low cost and potential for mass production. The cooling performance could be further enhanced to effectively reflect solar radiation and emit thermal radiation to the cold sky by designing microspheres suitable for PDRC applications. Hollow dielectric structures were numerically designed to enhance the PDRC performance of dielectric microsphere coatings. The maximum solar reflectance ($\overline{R}_{\text{solar}} = 0.96$) was obtained with a fill rate $f = 0.6$, outer radius $r_{\text{out}} = 0.5\ \mu\text{m}$, core–shell rate $\varphi = r_{\text{in}}/r_{\text{out}} = 0.3$, thickness $t = 300\ \mu\text{m}$, and thermal infrared emittance $\overline{\varepsilon}_{\text{LWIR}} = 0.90$. Furthermore, by controlling the multisize sphere distribution within $\varphi = 0.1$ to 0.5, the cooling performance at $t = 300\ \mu\text{m}$ was enhanced to $\overline{R}_{\text{solar}} = 0.98$, $\overline{\varepsilon}_{\text{LWIR}} = 0.95$, and a net cooling power of 77 W/m^2 was achieved at a temperature of 25°C, which was ~38% higher than that achieved with the single-size sphere coating ($\varphi = 0.3$) and ~64% higher than that of the solid SiO$_2$ sphere coating ($\varphi = 0$). These results indicate that hollow structures can effectively enhance the cooling performance of dielectric microsphere coatings by increasing the number of interfaces between the air and dielectric materials. © 2021 Society of Photo-Optical Instrumentation Engineers (SPIE) [DOI: 10.1117/1.JPE.11.042108]

Keywords: radiative cooling; dielectric; hollow sphere; solar reflectance; thermal emittance.

1 Introduction

The demand for cooling is rising as a result of global warming, population growth, industrial development, and higher living standards.[1] However, the current refrigeration process based on thermal cycles consumes a significant amount of energy, and the consumption of nonrenewable fossil energy increases carbon emissions, which contribute to global warming.[2] In addition, refrigerant emissions can cause new environmental problems, such as the greenhouse effect.[3] Therefore, the development of new ecofriendly cooling technologies has become an urgent issue.[4]

Passive daytime radiative cooling (PDRC) technology can be used to achieve energy-intensive cooling, which transfers excess heat to the outer space through thermal radiation without any energy consumption.[5–7] It uses a large temperature difference between the Earth (~300 K) and outer space (same as that of the black body radiation spectrum at 2.7 K[8,9]) and radiates infrared heat from the Earth's surface through the atmosphere to the outer space to achieve the cooling effect. The surface coating of a PDRC device must have a high solar reflectance ($\overline{R}_{\text{solar}}$) in the solar spectrum (0.3 to 2.5 μm) to avoid the solar heating, and a strong thermal emittance ($\overline{\varepsilon}_{\text{LWIR}}$) in the long-wave infrared (LWIR) transmission window (8 to 13 μm) of the atmosphere to lose heat to the cool sky. Thus, even during the day, the energy loss to the cold sky by thermal

---

radiation through the atmospheric LWIR window is significantly greater than that from sunlight; thus, electricity-free and spontaneous cooling is achieved.[10,11]

Recently, various PDRC coatings with high solar reflection and thermal LWIR emittance in the atmospheric window, such as photonic structures,[5] polymers,[12] dielectrics,[13,14] and dielectric-polymer composites,[15] have been developed. The intrinsic absorptance of polymer and dielectric materials can usually provide high emittance in the atmospheric LWIR window. Thus, to achieve near-perfect solar reflectance is significant to achieve PDRC. In the past decade, various strategies have been proposed to reflect solar radiation and achieve high-performance PDRC, including coating a bulk polymer on a highly solar reflective metal, such as Ag and Al,[16,17] and using porous or microsphere structures where the sphere interface, such as SiO_2–air, air–polymer, and SiO_2–polymer interfaces, amplifies the solar scattering.[18–21] Dielectric sphere-based radiative cooling coatings are gaining popularity owing to their low cost, potential for mass production, and applicability to large systems.[15] However, to achieve effective solar reflection, the coating must have a large thickness, or a solar reflector should be placed at the bottom of the PDRC device. By designing microspheres suitable for PDRC applications, cooling performance can be improved further to effectively reflect solar radiation and emit thermal radiation to the cold sky.

Therefore, hollow glass spheres[22] or hollow SiO_2 spheres[23] were prepared to enhance the solar reflectance using multiscattering interfaces. However, the relationship between the hollow sphere parameters and PDRC performance still needs to be clarified. In this study, hollow microsphere parameters, such as radius, core–shell ratio, fill rate, and thickness, were first discussed to clarify the relationship between these geometric parameters and the cooling performance. Then, a multitype sphere distribution was investigated to enhance the cooling performance of the dielectric sphere coating. Finally, the cooling powers of the hollow multitype microsphere coatings were calculated and compared with those of the solid microsphere and single-type microsphere coatings.

2 Concept and Model

2.1 Concept of Random Hollow Dielectric Microsphere Coating

Figure 1(a) shows the concept of a random hollow dielectric microsphere coating for PDRC. The outer and inner radii of the hollow sphere are r_{out} and r_{in}, respectively, with a core–shell ratio $\varphi = r_{in}/r_{out}$. The thickness and fill rate of the coating are defined as t and f (>0.55, owing to the random stacked structures).

To enhance the maximal net cooling performance during the day, the coating should have a value of $\overline{R}_{solar} = 1$ to reflect all solar radiation in the solar spectrum (0.3 to 2.5 μm) and $\overline{\varepsilon}_{LWIR} = 1$ to emit thermal radiation in the atmospheric LWIR transmittance window (8 to 13 μm). Thus, the bulk material used for this coating should be transparent without absorption in the solar spectrum and have a strong intrinsic absorption in the atmospheric LWIR window. Dielectric spheres (such as SiO_2) are excellent candidates for PDRC because they have strong scattering abilities in the UV–visible light region and large emittance in the infrared region owing to their intrinsic absorptance. Figure 1(b) shows the refractive indices of SiO_2 based
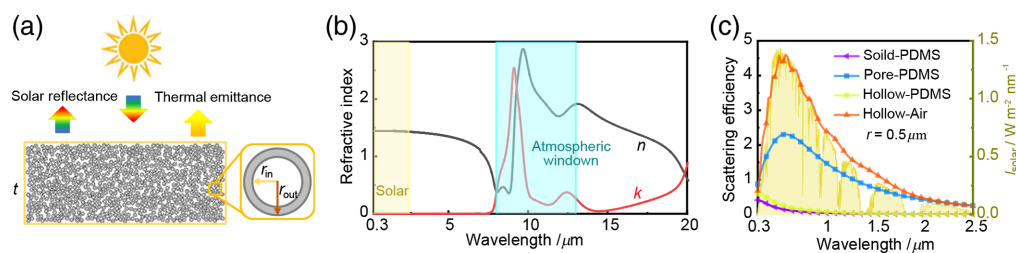

Fig. 1 (a) Concept of the random hollow dielectric microsphere coating to reflect solar radiation and emit infrared thermal radiation. (b) Refractive indices (0.3 to 20 μm) of SiO_2 based on the previous studies.[24,25] (c) Scattering efficiency of SiO_2 sphere, pore, and hollow SiO_2 sphere ($r = 0.5$ μm) in different dielectric environments (air or PDMS).

on previous studies,[24,25] and it can be observed that the bulk SiO_2 material exhibits minimal absorption in the solar spectrum, although it exhibits strong absorptance in the atmospheric window.

To further understand the effect of single sphere (solid or hollow) and dispersed dielectric environment (polymer or air) on the scattering performance, the scattering efficiency of the single microsphere was calculated in Fig. 1(c). Electromagnetic (EM) field propagation around a single sphere can be described by the Helmholtz equation, which can be solved by finite element method (FEM):

$$\nabla \times (\mu_r^{-1} \nabla \times \mathbf{E}) - k_0^2 \epsilon_r \mathbf{E} = 0, \tag{1}$$

where $\mathbf{E}$ is the electric field of the medium; μ_r is the relative magnetic permeability; k_0 is the wave number; ϵ_r is the relative dielectric function, which is calculated as $\epsilon_r = (n - i\kappa)^2$; n and κ are the complex refractive indices. The scattering power can be obtained by the Poynting vector. More detail of FEM can be found in the previous works.[26,27,28]

It can be identified that a polymer matrix, such as PDMS, with a similar refractive index as SiO_2 (1.39 versus 1.44)[29] would weaken the scattering performance of SiO_2 spheres in the polymer ($SiO_2 - PDMS$) in the solar spectrum. The hollow sphere in the polymer ($air@SiO_2 - PDMS$) can slightly enhance the scattering ability of the sphere, which is still much lower than that of the porous polymer structure (air–PDMS). However, a hollow sphere in air can achieve a stronger scattering ability in the solar spectrum owing to the presence of multiple interfaces with different refractive indices, which can increase the reflectivity or scattering probability of photons and enable the realization of a higher solar reflectance. Therefore, in this study, hollow SiO_2 microspheres randomly distributed in the air were selected as the PDRC coating, and the sphere fill rate was >0.55 so that a sphere-stacked structure could be achieved.[18,30]

2.2 Simulation Model of the Microsphere Coating

The microsphere coating with an outer radius r_{out} was built by randomly distributing spheres (N) in a square (width w and thickness t). The position of microsphere was first determined by a random number. Then, it would be further restricted to ensure that the sphere is in connect with at least on existing spheres since spheres are stacked together. The fill rate f and effective thickness t_e were determined as

$$f = \frac{N\pi r_{out}^2}{wt}, \tag{2}$$

$$t_e = \frac{N\pi r_{out}^2}{w} = ft, \tag{3}$$

where t_e is the thickness of a nonporous solid film with the same amount of materials as the porous film to study.

Direct three-dimensional (3D) simulation of microsphere coatings is extremely expensive due to its nonrepeatable nature. For example, with a volume of $10 \times 10 \times 100 \ \mu m^3$ and a mesh size of ~10 nm, the mesh number reaches ~10 billions, which is very challenging to solve. Hence, a two-dimensional (2D) simulation based on FEM was conducted to reduce the computational load, which is expected to capture key features in 3D light scattering, since individual 2D and 3D pores show similar scattering efficiency as a function of pore radius at different wavelengths, suggesting that the optimal pore sizes for $\overline{R}_{solar}$, $\overline{\varepsilon}_{LWIR}$, and radiative cooling should be similar in 2D and 3D.[31]

To simplify the simulation, periodic boundary conditions are used at the left and right sides. A plane wave is excited from the port on the top side of the unit cell with a power of 1 W. EM transfer equation can be solved by FEM using nonhomogeneous Helmholtz equation in Eq. (1). The reflected and transmitted powers can be monitored by integrating from the bottom and top ports. The absorbed power can be achieved by integrating the heat power density with the coating. More details and model verification can be found in our previous studies.[32,33]

Finally, the emittance ε (i.e., absorptance A), reflectance R, and transmittance τ can be calculated using the absorbed, reflected, and transmitted power, respectively, divided by the incident power.

The solar reflectance ($\overline{R}_{\text{solar}}$) can be calculated as the ratio of the reflected solar intensity across the solar spectrum ($\lambda = 0.3$ to 2.5 μm), as

$$\overline{R}_{\text{solar}} = \frac{\int_{0.3\ \mu m}^{2.5\ \mu m} I_{\text{solar}}(\lambda) R(\lambda) d\lambda}{\int_{0.3\ \mu m}^{2.5\ \mu m} I_{\text{solar}}(\lambda) d\lambda}, \tag{4}$$

where $I_{\text{solar}}(\lambda)$ represents the ASTM G173-03 global solar intensity spectrum at AM 1.5 and $R(\lambda)$ represents the spectral reflectance of the coating.

Similarly, the thermal emittance $\overline{\varepsilon}_{\text{LWIR}}$ is expressed as follows:

$$\overline{\varepsilon}_{\text{LWIR}} = \frac{\int_{8\ \mu m}^{13\ \mu m} I_{\text{bb}}(T, \lambda) \varepsilon(T, \lambda) d\lambda}{\int_{8\ \mu m}^{13\ \mu m} I_{\text{bb}}(T, \lambda) d\lambda}, \tag{5}$$

where $I_{\text{bb}}(T, \lambda)$ represents the spectral intensity emitted by a standard blackbody with a temperature of T, and $\varepsilon(T, \lambda)$ represents the spectral emittance of the coating.

Due to computational load, the directional reflectance or emittance is used to calculate the cooling performance since reflectance or emittance does not depend on angle in a wide region, which can be verified by simulation data or experimental results.[12,31,34] When the coating is exposed to a daytime sky, it is subject to both solar radiation and atmospheric thermal radiation (corresponding to the ambient air temperature T_{atm}). The net cooling power $P_{\text{cool}}(T)$ of such a radiative cooler is provided without the consideration of the thermal convection and conductivity:[5]

$$P_{\text{cool}}(T) = P_{\text{rad}}(T) - P_{\text{atm}}(T_{\text{atm}}) - P_{\text{sun}}, \tag{6}$$

where $P_{\text{rad}}(T)$, $P_{\text{atm}}(T_{\text{atm}})$, and P_{sun} represent the radiation power, absorbed power from the incident atmospheric irradiation, and solar irradiation, respectively, which can be integrated based on the emittance of the coating and the radiative power of the blackbody.[5,31] $T = T_{\text{atm}} = 25$°C was considered for the cooling power calculation.

3 Results and Discussion

To achieve a high solar reflectance, a thickness of ~300 μm is usually required; such a thickness would require more computational load. In addition, $\overline{R}_{\text{solar}}$ and $\overline{\varepsilon}_{\text{LWIR}}$ increase monotonically with thickness.[31] Thus, a thickness of 20 μm was used to investigate the effect of different parameters (core–shell ratio, sphere radius, fill ratio, and size distribution), and the cooling performance was evaluated at 300 μm.

3.1 Effect of Core–Shell Ratio on the Cooling Performance

For the hollow structure, the effect of the core–shell ratio $\varphi = r_{\text{in}}/r_{\text{out}}$ on the cooling performance is shown in Fig. 2. First, the scattering properties of a single hollow sphere were calculated, as shown in Fig. 2(a), where the scattering region becomes narrow and shows a blueshift tendency with increasing φ in the solar spectrum. The reflectance spectrum of the coating becomes narrow with strong peaks with increasing φ in the solar spectrum, and the maximum $\overline{R}_{\text{solar}}$ can be achieved as 0.58 at $\varphi = 0.3$ [Figs. 2(b) and 2(d)]. While the emittance spectrum is similar at small values (0 to 0.4) of φ, the emittance region becomes narrow and the peaks become weak when φ increases from 0.5 to 1.0, resulting in slight changes in $\overline{\varepsilon}_{\text{LWIR}}$ (~0.86) when $\varphi = 0$ to 0.4; however, $\overline{\varepsilon}_{\text{LWIR}}$ drops rapidly from 0.85 to 0.33, when φ increases from 0.5 to 1.0 [Figs. 2(c) and 2(d)]. Therefore, φ can be selected as 0.3 to achieve the maximum solar reflectance, although the thermal LWIR emittance changes slightly at this value (Fig. 2).
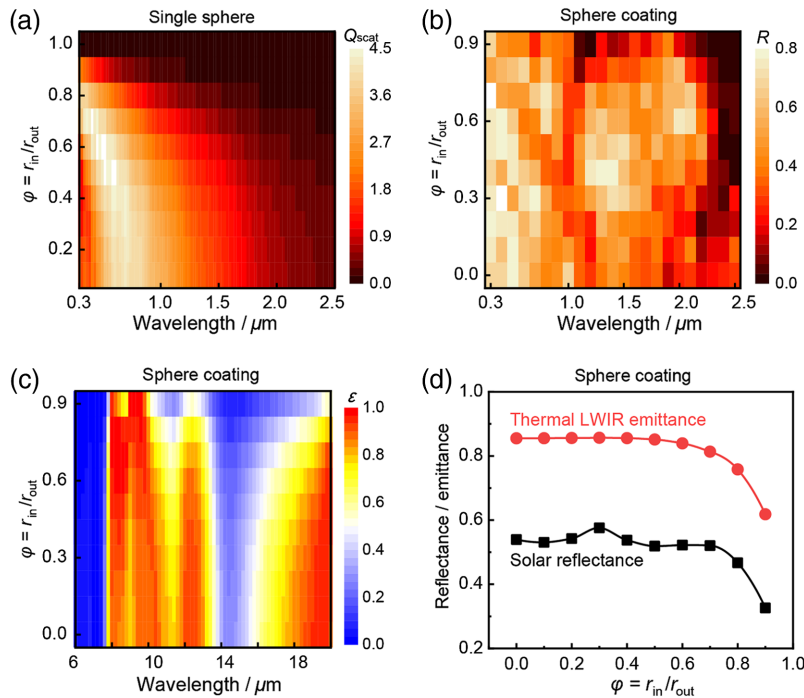
Fig. 2 Effect of $\varphi = r_{in}/r_{out}$ on the cooling performance for random hollow microsphere coatings. (a) Scattering efficiencies of a SiO_2 microsphere with different φ in air. (b) Simulated reflectance spectra of microsphere coatings with different φ in the solar spectrum ($\lambda = 0.3$ to 2.5 μm). (c) Simulated emittance (i.e., absorptance) spectra of microsphere coatings with different φ in the infrared region ($\lambda = 6$ to 20 μm). (d) Calculated $\overline{R}_{solar}$ and $\overline{\varepsilon}_{LWIR}$ with different φ. (b)–(d) $r_{out} = 0.5$ μm, $f = 0.6$, and $t = 20$ μm.

3.2 Effect of Sphere Radius on the Cooling Performance

In PDRC applications, the sphere radius (r_{out}) is critical for reflecting solar radiation. Thus, the effect of the sphere radius on cooling performance was investigated. According to the Mie scattering theory, for a single sphere, the scattering peak usually undergoes a redshift with increasing sphere size. For random microsphere coatings, increasing r_{out} would also lead to a redshift of the reflectance spectrum, as shown in Fig. 3(a). The emittance (i.e., absorptance) spectrum is almost the same when r_{out} ranges from 0.1 to 0.5 μm, as shown in Fig. 3(b).

The larger value of r_{out} would also lead to a small change in the emittance spectra. Therefore, based on the solar radiation spectrum (0.3 to 2.5 μm) and atmosphere transmission spectrum (8 to 13 μm), the calculated $\overline{\varepsilon}_{LWIR}$ changes minimally, ranging between 0.84 and 0.89, whereas
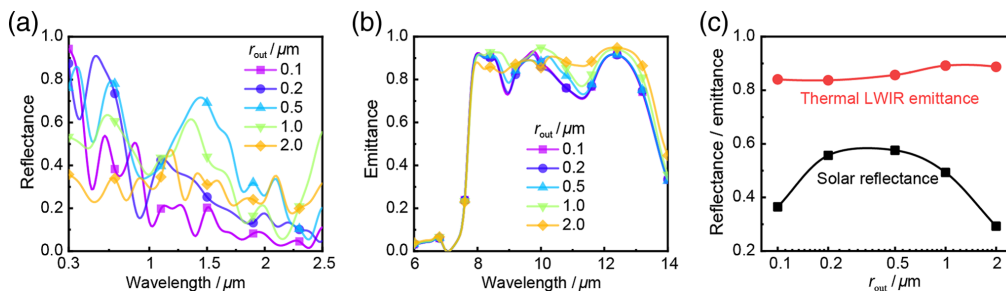

Fig. 3 Effect of microsphere radius r_{out} (0.1 to 2 μm) on the cooling performance for random hollow microsphere coatings. (a) Simulated reflectance spectra of microsphere coatings with different r_{out} in the solar spectrum ($\lambda = 0.3$ to 2.5 μm). (b) Simulated emittance (i.e., absorptance) spectra of microsphere coatings with different r_{out} in the infrared region ($\lambda = 6$ to 14 μm). (c) Calculated $\overline{R}_{solar}$ and $\overline{\varepsilon}_{LWIR}$ with different sphere radii. $\varphi = r_{in}/r_{out} = 0.3$, $f = 0.6$, and $t = 20$ μm.
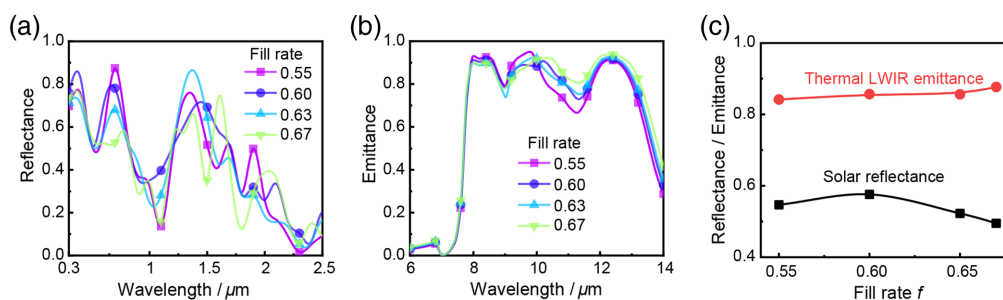
Fig. 4 Effect of the microsphere fill rate f (0.55 to 0.67) on the cooling performance for random hollow microsphere coatings. (a) Simulated reflectance spectra of microsphere coating with different f in the solar spectrum ($\lambda = 0.3$ to 2.5 μm). (b) Simulated emittance (i.e., absorptance) spectra of microsphere coating with different f in the infrared region ($\lambda = 6$ to 14 μm). (c) Calculated $\overline{R}_{solar}$ and $\overline{\varepsilon}_{LWIR}$ with different fill rates. $\varphi = r_{in}/r_{out} = 0.3$, $r_{out} = 0.5$ μm, and $t = 20$ μm.

$\overline{R}_{solar}$ first increases from 0.37 to 0.58 when r increases from 0.1 to 0.5 μm and then drops to 0.29 at $r_{out} = 2$ μm, as shown in Fig. 2(c). The sphere radius in this region has a minimal effect on $\overline{\varepsilon}_{LWIR}$, which is mainly determined by the effective thickness of the bulk SiO_2 material because the size of the sphere is much smaller than the infrared wavelength (8 to 13 μm). Because solar radiation mainly occurs in the 0.3 to 1.5 μm wavelength range, the reflectance spectrum of the SiO_2 coating with the sphere $r_{out} = 0.5$ μm matches well with the solar spectrum. Furthermore, this coating achieves the largest $\overline{R}_{solar} = 0.58$ at $t = 20$ μm, and its $\overline{\varepsilon}_{LWIR}$ is as large as 0.86. Therefore, to enhance the solar reflectance while maintaining a high thermal emittance in the atmosphere LWIR transmission window, an optimal outer sphere radius of 0.5 μm should be used.

3.3 Effect of Sphere Filling Rate on the Cooling Performance

The fill rate (f) is another critical parameter of the random stacked structure and should be determined for PDRC applications. Because f in this stacked structure increases from 0.6 to 0.67, the cavity between the spheres reduces, and more photons can be transmitted with less travel length, leading to a decrease in reflectance in the solar spectrum ($\lambda = 0.3$ to 2.5 μm), as shown in Fig. 4(a). On the one hand, increasing f would slightly improve the emittance in the infrared region ($\lambda = 8$ to 13 μm), as shown in Fig. 4(b), resulting in a gradual increase in $\overline{\varepsilon}_{LWIR}$ from 0.84 to 0.88 when f increases from 0.55 to 0.76. On the other hand, $\overline{R}_{solar}$ increases slightly from 0.55 to 0.58, when f increases from 0.55 to 0.60, and then drops to 0.49, at $f = 0.76$, [Fig. 4(c)]. Therefore, to balance $\overline{R}_{solar}$ and $\overline{\varepsilon}_{LWIR}$, f can be optimized to 0.60 to achieve the maximum $\overline{R}_{solar} = 0.58$, whereas $\overline{\varepsilon}_{LWIR} = 0.86$ only decreases slightly.

3.4 Effect of Thickness on the Cooling Performance

As discussed earlier, a thickness of 20 μm was used to investigate the effect of different parameters (core–shell ratio, sphere radius, fill ratio, and size distribution) by reducing the computation load. In this section, three thicknesses (20, 40, and 60 μm) in Fig. 5 are first calculated to justify it. It can be found that the dependences of $\overline{R}_{solar}$ and $\overline{\varepsilon}_{LWIR}$ on r_{out} and fill rate are the same at different thicknesses. Therefore, the results at a thickness of 20 μm can be extended to thicker films.

    Based on the optimal r and f derived above ($\varphi = 0.3$, $r_{out} = 0.5$ μm, and $f = 0.6$), the thickness (t) of the coating should be determined. With increasing t, the probability of incident photons being scattered by the hollow sphere would be enhanced, resulting in enhanced reflectance in the solar spectrum ($\lambda = 0.3$ to 2.5 μm) [Fig. 6(a)]. In addition, a large t would further increase the effective thickness of the bulk SiO_2 material, leading to enhanced emittance in the infrared region ($\lambda = 6.0$ to 14 μm), as shown in Fig. 6(b). Hence, both $\overline{R}_{solar}$ and $\overline{\varepsilon}_{LWIR}$ increase rapidly from 0.366 to 0.840 and 0.726 to 0.959, respectively, when t increases from 10 to 100 μm;
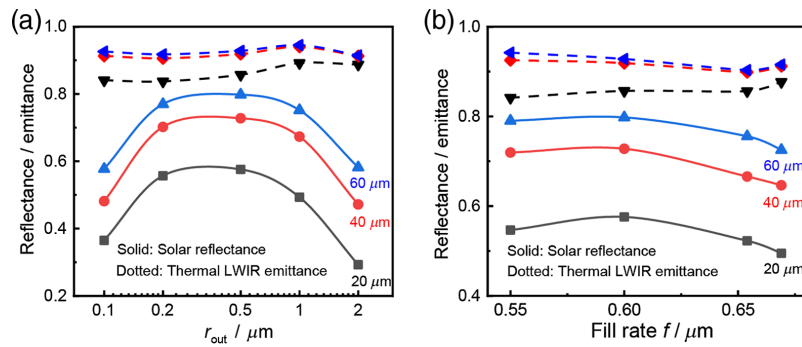
Fig. 5 Calculated $\overline{R}_{solar}$ and $\overline{\varepsilon}_{LWIR}$ with different outer radii (a) r_{out} and (b) fill rates f at thicknesses of 20, 40, and 60 μm. (a) $\varphi = r_{in}/r_{out} = 0.3$, and $f = 0.6$; (b) $\varphi = r_{in}/r_{out} = 0.3$, and $r_{out} = 0.5$ μm.
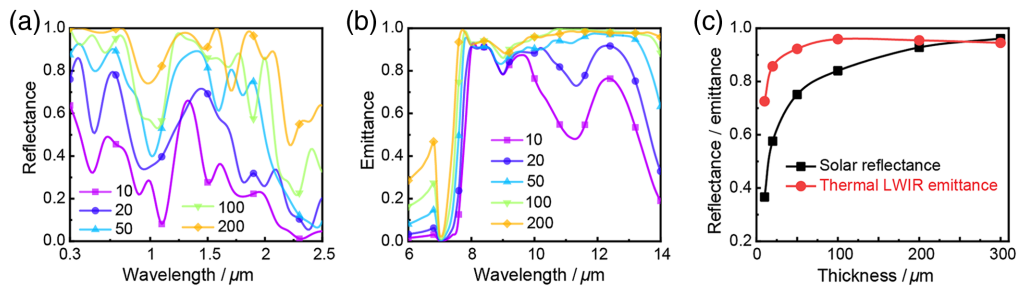

Fig. 6 Effect of thicknesses (0 to 300 μm) on the cooling performance for hollow SiO$_2$ coatings. (a) Simulated reflectance spectra of coatings with different thicknesses in the solar spectrum ($\lambda = 0.3$ to 2.5 μm). (b) Simulated emittance spectra of coatings with different thicknesses in the infrared region ($\lambda = 6.0$ to 14 μm). (d) Calculated $\overline{R}_{solar}$ and $\overline{\varepsilon}_{LWIR}$ with different thicknesses. $\varphi = r_{in}/r_{out} = 0.3$, $r_{out} = 0.5$ μm and $f = 0.6$.

then, $\overline{R}_{solar}$ increases slowly to 0.961, and $\overline{\varepsilon}_{LWIR}$ decreases slightly to 0.945 at $t = 300$ μm, as shown in Fig. 6(c). Therefore, to balance the cooling performance and material cost, the thickness t at 200 to 300 μm is better based on the hollow SiO$_2$ sphere coating.

3.5 *Effect of Sphere Radius Distribution on the Cooling Performance*

The above studies focused on single-size spheres; however, spheres with different size distributions may further enhance the cooling performance. A small dielectric sphere can effectively scatter or reflect ultraviolet light, and large spheres can scatter more light at longer wavelengths. On the contrary, hollow dielectric spheres with different φ values also exhibit different scattering performances in the solar spectrum, as shown in Fig. 2(a). Thus, tuning the sphere size or core–shell ratio distribution by mixing different spheres may be used to enhance $\overline{R}_{solar}$. Under these conditions, $\overline{\varepsilon}_{LWIR}$ would not weaken because it is mainly determined by the effective thickness of the bulk SiO$_2$ material. Therefore, coatings with different spheres were considered. The total fill rate of the hollow sphere was set to 0.6, and the different blending fill rates were tuned to understand the effect of sphere size or core–shell ratio distribution on the cooling performance (Figs. 7 and 8).

First, two kinds of spheres ($\varphi = r_{in}/r_{out} = 0.3$) with $r_{out} = 0.2$ and 0.5 μm were investigated [Figs. 7(a)–7(c)]. Because the fill rate of the sphere ($r = 0.5$ μm)$f_r = 0.5$ was increased, the reflectance in the ultraviolet region of 0.3 to 0.4 μm increased gradually, owing to a decrease in the fraction of spheres with $r = 0.2$ μm or $f_r = 0.2$, as shown in Fig. 3(a); however, the reflectance in the visible region increased as more spheres with $r_{out} = 0.2$ μm could scatter light in this region [Fig. 3(a)]. However, the reflectance at 1.1 to 1.8 μm decreased with increasing $f_r = 0.2$, as shown in Fig. 7(a). Thus, $\overline{R}_{solar}$ is similar, located within the 0.56 to 0.58 range.
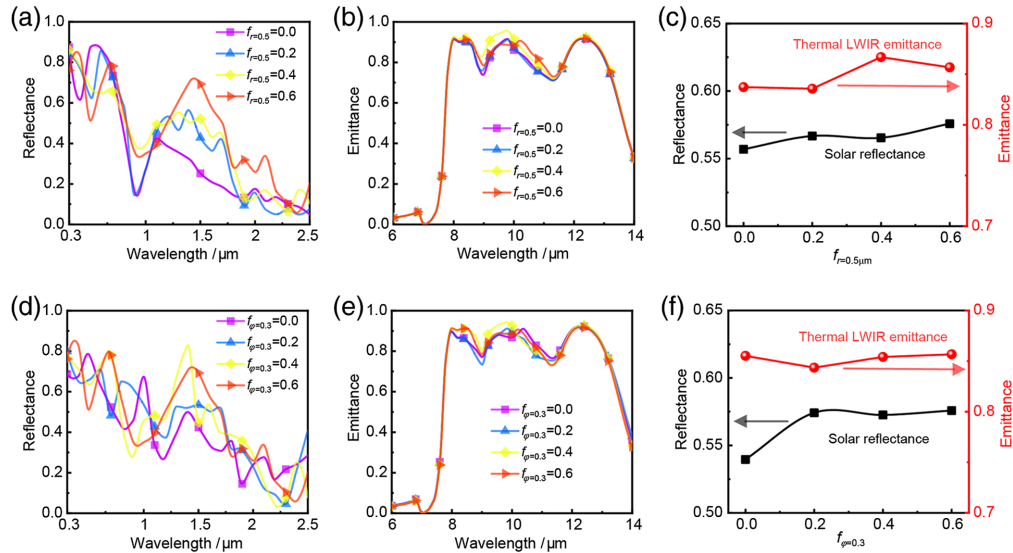
Fig. 7 (a)–(c) Effect of two-size spheres ($\varphi = r_{in}/r_{out} = 0.3$) with two different outer radii (0.2 and 0.5 μm) on the cooling performance of hollow SiO$_2$ coatings. (a) Simulated reflectance ($\lambda = 0.3$ to 2.5 μm) and (b) emittance ($\lambda = 6$ to 14 μm) of coatings with different fill rates of these two spheres in the simulated spectrum. (c) Calculated $\overline{R}_{solar}$ and $\overline{\varepsilon}_{LWIR}$ based on (a) and (b). (d)–(f) Effect of two-size spheres ($r_{out} = 0.5$ μm) with two different core–shell rates ($\varphi = r_{in}/r_{out} = 0.3$ and $\varphi = r_{in}/r_{out} = 0$) on the cooling performance for SiO$_2$ coatings. (d) Simulated reflectance ($\lambda = 0.3$ to 2.5 μm) and (e) emittance ($\lambda = 6$ to 14 μm) of coatings with different fill rates of these two spheres in the simulated spectrum. (f) Calculated $\overline{R}_{solar}$ and $\overline{\varepsilon}_{LWIR}$ based on (d) and (e). $t = 20$ μm and total $f = 0.6$.

Because the total fill rate of these two spheres was constant (0.6) based on the above studies, the emittance spectrum was almost the same for different blending fill rates [Fig. 7(b)], which agrees with the above discussion regarding the thermal emittance. Thus, tuning the fill rate distribution at the same total fill rate has a small effect on $\overline{\varepsilon}_{LWIR}$, which remains 0.84 to 0.87, as shown in Fig. 7(c).

Second, two different spheres ($r_{out} = 0.5$ μm) with $\varphi = r_{in}/r_{out} = 0$ and 0.3 were also considered [Figs. 7(d)–7(f)]. The reflectance spectra exhibit a similar tendency, and $\overline{R}_{solar}$ increases slightly from 0.54 to 0.58 when $f_{\varphi=0.3}$ increases from 0 to 0.6, indicating that the hollow structure can reflect solar radiation effectively. The emittance spectra are also similar, resulting in small variations in $\overline{\varepsilon}_{LWIR}$ (0.84 to 0.86). As discussed above, it was identified that mixing two kinds of spheres with different sizes or core–shell ratios have a minimal effect on $\overline{R}_{solar}$ and $\overline{\varepsilon}_{LWIR}$, and better cooling performance at $t = 20$ μm can be achieved as $\overline{R}_{solar} = 0.58$ and $\overline{\varepsilon}_{LWIR} = 0.86$ for single-size hollow spheres with $r_{out} = 0.5$ μm, $\varphi = r_{in}/r_{out} = 0.3$, and $f = 0.6$.

To further understand the effect of the outer radius r_{out} and core–shell ratio φ distributions on the cooling performance, Gaussian distribution $N(\mu, \sigma^2)$ of r_{out} and φ are first calculated in Fig. 8, where μ and σ are the expectation and standard deviation for r_{out} or φ. It can be found that Gaussian distribution of r_{out} with a larger σ would weaken $\overline{R}_{solar}$ while enhancing $\overline{\varepsilon}_{LWIR}$ slightly, which is also similar to the effect of Gaussian distribution φ. At the optimal $r_{out} = 0.5$ μm and $\varphi = 0.3$, the small fluctuations (i.e., $\sigma \leq 0.05$) have little effect on $\overline{R}_{solar}$ and $\overline{\varepsilon}_{LWIR}$ in Fig. 8, indicating the optimal result is acceptable in the practical scenario.

In addition, a random uniform distribution of φ within a certain region in the coating is considered for $r_{out} = 0.5$ μm, $t = 20$ μm, and $f = 0.6$, as shown in Fig. 9. First, one end of the random φ distribution was set as 0.3 in Figs. 9(a)–9(c). As φ in the region approaches 0.3, $\overline{R}_{solar}$ gradually increases while $\overline{\varepsilon}_{LWIR}$ remains almost the same (0.86 to 0.88), indicating that the hollow dielectric sphere with $\varphi = 0.3$ is better for reflecting solar radiation, which agrees well with the results discussed φ in Sec. 3.1. Thus, to enhance solar reflectance, the center of the
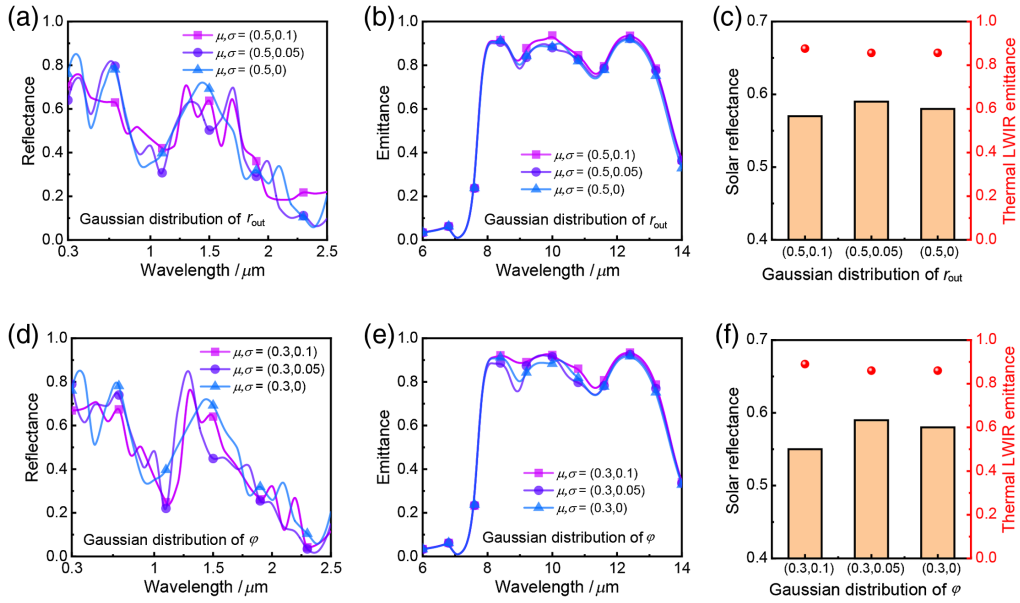
Fig. 8 (a)–(c) Effect of Gaussian distribution $N(\mu, \sigma^2)$ of the outer radius r_{out} on the cooling performance ($\mu = r_{out} = 0.5\ \mu m$, $\varphi = 0.3$). (a) Simulated reflectance ($\lambda = 0.3$ to $2.5\ \mu m$) and (b) emittance ($\lambda = 6$ to $14\ \mu m$) of coatings with different standard deviations σ. (c) Calculated $\overline{R}_{solar}$ and $\overline{\varepsilon}_{LWIR}$ based on (a) and (b). (d)–(f) Effect of Gaussian distribution $N(\mu, \sigma^2)$ of the core–shell ratio φ on the cooling performance ($\mu = \varphi = 0.3$, $r_{out} = 0.5\ \mu m$). (a) Simulated reflectance ($\lambda = 0.3$ to $2.5\ \mu m$) and (b) emittance ($\lambda = 6$ to $14\ \mu m$) of coatings with different standard deviations σ. (c) Calculated $\overline{R}_{solar}$ and $\overline{\varepsilon}_{LWIR}$ based on (a) and (b). $t = 20\ \mu m$, and total $f = 0.6$.
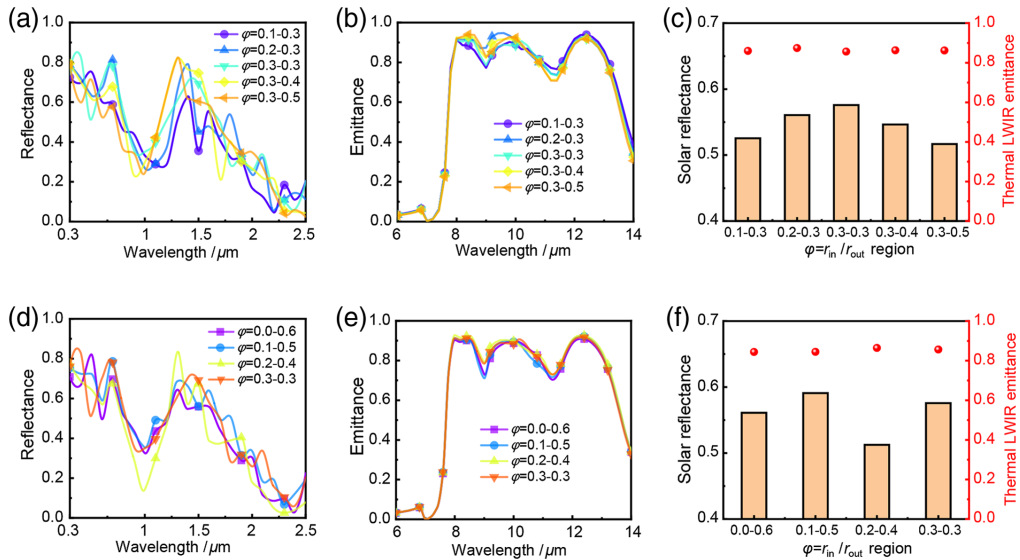

Fig. 9 Uniform distributions of the core–shell ratio φ: (a)–(c) effect of multisize spheres with different random uniform distributions of the core–shell ratio φ (one end of the range is set as $\varphi = 0.3$) on the cooling performance of hollow SiO_2 coatings. (a) Simulated reflectance ($\lambda = 0.3$ to $2.5\ \mu m$) and (b) emittance ($\lambda = 6$ to $14\ \mu m$) of coatings with different fill rates of these two spheres in the simulated spectrum. (c) Calculated $\overline{R}_{solar}$ and $\overline{\varepsilon}_{LWIR}$ based on (a) and (b). (d)–(f) Effect of multisize spheres with different random uniform distributions of the core–shell ratio φ (the center of the range is set as $\varphi = 0.3$) on the cooling performance of SiO_2 coatings. (d) Simulated reflectance ($\lambda = 0.3$ to $2.5\ \mu m$) and (e) emittance ($\lambda = 6$ to $14\ \mu m$) of coatings with different fill rates of these two spheres in the simulated spectrum. (f) Calculated $\overline{R}_{solar}$ and $\overline{\varepsilon}_{LWIR}$ based on (d) and (e). $r_{out} = 0.5\ \mu m$, $t = 20\ \mu m$, and total $f = 0.6$.

region with random distributions of φ was set to 0.3 [Figs. 9(d)–9(f)]. The results revealed that the maximum $\overline{R}_{solar}$ that can be achieved is 0.59, in the range of $\varphi = 0.1$ to 0.5, and $\overline{\varepsilon}_{LWIR}$ is almost the same (0.84 to 0.87).

3.6 *Net Cooling Power for Optimized Microsphere Coating*

As discussed above, the thickness considered is small, resulting in a small value of $\overline{R}_{solar}\,\overline{\varepsilon}_{LWIR}$. Thus, a thicker coating with $t = 300\ \mu m$ was calculated based on the optimal sphere with a multicore–shell ratio ($\varphi = 0.1$ to 0.5) and compared to that of the sphere with a single core–shell ratio ($\varphi = 0.3$) (Fig. 10). In the solar spectrum, the hollow sphere coating with multi-φ has better reflectance performance in the solar spectrum than a single-φ hollow sphere coating [Fig. 10(a)], which agrees well with the findings shown in Fig. 9. However, in the thermal LWIR spectrum, the emittance of the multihollow φ sphere coating was higher than that of the single-φ hollow sphere coating, as shown in Fig. 10(b). Thus, and of the multisphere φ coating are 0.98 and 0.95, respectively, which are higher than those of the single-sphere φ coating ($\overline{R}_{solar} = 0.96$ and $\overline{\varepsilon}_{LWIR} = 0.90$) and solid sphere coating ($\overline{R}_{solar} = 0.95$ and $\overline{\varepsilon}_{LWIR} = 0.92$), indicating that the optimal hollow sphere coating with the multicore–shell ratio exhibits a better performance.

However, for the bulk sphere coating discussed above, the transmittance is not zero at $t = 300\ \mu m$. To conservatively evaluate the cooling performance of the bulk coating without the substrate, the reflectance spectrum was used to calculate the solar heating power P_{sun}, and the emittance spectrum was used to calculate the radiation power from the coating to the sky P_{rad} and the radiation from the atmosphere to the coating P_{atm}. Thus, under typical atmospheric conditions and the standard AM 1.5 solar spectrum, the net cooling power of the solid sphere ($\varphi = 0$) coating is $P_{cool} = P_{rad} - P_{sun} - P_{atm} = 47\ W/m^2$. The hollow sphere with $\varphi = 0.3$ further enhanced the net cooling power to $P_{cool} = 56\ W/m^2$. Finally, the maximum P_{cool} was 77 W/m^2 for the hollow SiO_2 microsphere coating with $\varphi = 0.1$ to 0.5, as shown in Table 1. These results indicate that a random hollow dielectric microsphere coating can be used to achieve effective radiative cooling performance.
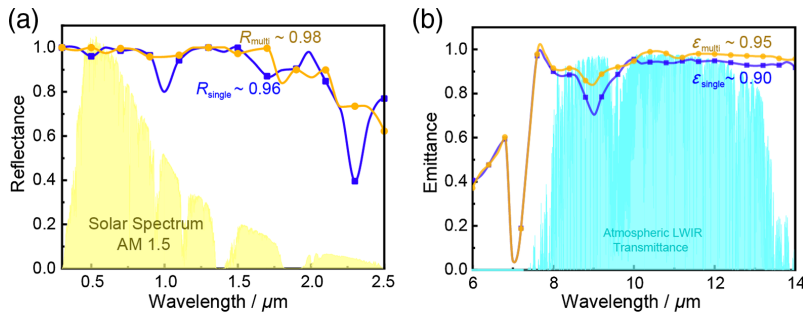

Fig. 10 Cooling performance for the optimized hollow SiO_2 microsphere coatings. (a) Simulated reflectance and (b) emittance spectra of microsphere coatings without substrate. $t = 300\ \mu m$, $r_{out} = 0.5\ \mu m$, and total $f = 0.6$.

Table 1 Cooling powers of hollow microsphere coatings with different core–shell ratios at $T = 25°C$, $t = 300\ \mu m$, $r_{out} = 0.5\ \mu m$, and total $f = 0.6$.

Sphere ($r_{out} = 0.5\ \mu m$)	P_{rad}	P_{sun}	P_{atm}	P_{net}
$\varphi = 0$ (solid)	285	46	192	47
$\varphi = 0.3$ (single)	279	35	188	56
$\varphi = 0.1$ to 0.5 (multi)	288	19	192	77

4 Conclusion

In summary, a hollow dielectric structure was introduced to enhance the daytime cooling performance of a dielectric sphere coating. It can be observed that the hollow dielectric sphere in air can scatter more light in the solar spectrum. For the single-size hollow sphere coating, it can be observed that the maximum $\overline{R}_{\text{solar}}$ can be achieved at $f = 0.6$, $r_{\text{out}} = 0.5$ μm, and $\varphi = r_{\text{in}}/r_{\text{out}} = 0.3$, whereas $\overline{\varepsilon}_{\text{LWIR}}$ changes little because of the small size compared with the infrared wavelength. Increasing the thickness of the hollow microsphere coating based on the single-size hollow sphere coating can enhance both $\overline{R}_{\text{solar}}$ and $\overline{\varepsilon}_{\text{LWIR}}$ while gradually reaching saturation. Thus, the radiative cooling performance based on single-size sphere coating can be obtained as $\overline{R}_{\text{solar}} = 0.96$ and $\overline{\varepsilon}_{\text{LWIR}} = 0.90$, when $t = 300$ μm. Furthermore, by controlling the core–shell ratio distribution, the cooling performance of bulk coatings ($t = 300$ μm) can be enhanced to $\overline{R}_{\text{solar}} = 0.98$ and $\overline{\varepsilon}_{\text{LWIR}} = 0.95$, when $\varphi = 0.1$ to 0.5, resulting in a net cooling power of 77 W/m^2, which is $\sim$38% higher than that of the optimal single-size hollow sphere coating ($\varphi = 0.3$), and $\sim$64% higher than that of the optimal solid SiO$_2$ sphere coating ($\varphi = 0$). These results indicate that the hollow structure can effectively enhance the cooling performance of dielectric microsphere coatings by increasing the number of interfaces between the air and dielectric.

Acknowledgments

Code, Data, and Materials Availability

The data that support the findings of this study are available upon reasonable request from the authors.

References

1. M. Isaac and D. P. van Vuuren, "Modeling global residential sector energy demand for heating and air conditioning in the context of climate change," *Energy Policy* **37**(2), 507–521 (2009).
2. J. Henley, "World set to use more energy for cooling than heating," *The Guardian*, 26 October 2015, https://www.theguardian.com/environment/2015/oct/26/cold-economy-cop21-global-warming-carbon-emissions (2015).
3. J. Steven Brown and P. A. Domanski, "Review of alternative cooling technologies," *Appl. Therm. Eng.* **64**(1–2), 252–262 (2014).
4. J. Chen et al., "Development of a new spectral selectivity-based passive radiative roof cooling model and its application in hot and humid region," *J. Clean. Prod.* **307**, 127170 (2021).
5. A. P. Raman et al., "Passive radiative cooling below ambient air temperature under direct sunlight," *Nature* **515**(7528), 540–544 (2014).
6. J. Liu et al., "Research on the performance of radiative cooling and solar heating coupling module to direct control indoor temperature," *Energy Convers. Manag.* **205**, 112395 (2020).
7. W. Huang et al., "Scalable aqueous processing-based passive daytime radiative cooling coatings," *Adv. Funct. Mater.* **31**, 2010334 (2021).
8. D. J. Fixsen, "The temperature of the cosmic microwave background," *Astrophys. J.* **707**(2), 916–920 (2009).
9. B. Zhao et al., "Radiative cooling: a review of fundamentals, materials, applications, and prospects," *Appl. Energy* **236**, 489–513 (2019).
10. D. Zhao et al., "Radiative sky cooling: fundamental principles, materials, and applications," *Appl. Phys. Rev.* **6**(2), 021306 (2019).
11. J. Liu et al., "Field investigation and performance evaluation of sub-ambient radiative cooling in low latitude seaside," *Renew. Energy* **155**, 90–99 (2020).

12. J. Mandal et al., "Hierarchically porous polymer coatings for highly efficient passive daytime radiative cooling," *Science* **362**(6412), 315–319 (2018).
13. S. Y. Jeong et al., "Field investigation of a photonic multi-layered TiO$_2$ passive radiative cooler in sub-tropical climate," *Renew. Energy* **146**, 44–55 (2020).
14. R. A. Yalçın et al., "Daytime radiative cooling with silica fiber network," *Sol. Energy Mater. Sol. Cells* **206**, 110320 (2020).
15. Y. Zhai et al., "Scalable-manufactured randomized glass-polymer hybrid metamaterial for daytime radiative cooling," *Science* **355**(6329), 1062–1066 (2017).
16. E. Rephaeli, A. Raman, and S. Fan, "Ultrabroadband photonic structures to achieve high-performance daytime radiative cooling," *Nano Lett.* **13**(4), 1457–1461 (2013).
17. Z. Chen et al., "Radiative cooling to deep sub-freezing temperatures through a 24-h day-night cycle," *Nat. Commun.* **7**, 13729 (2016).
18. S. Atiganyanun et al., "Effective radiative cooling by paint-format microsphere-based photonic random media," *ACS Photonics* **5**(4), 1181–1187 (2018).
19. H. Bao et al., "Double-layer nanoparticle-based coatings for efficient terrestrial radiative cooling," *Sol. Energy Mater. Sol. Cells* **168**, 78–84 (2017).
20. Y. Chen et al., "Colored and paintable bilayer coatings with high solar-infrared reflectance for efficient cooling," *Sci. Adv.* **6**(17), eaaz5413 (2020).
21. Z. Huang and X. Ruan, "Nanoparticle embedded double-layer coating for daytime radiative cooling," *Int. J. Heat Mass Transf.* **104**, 890–896 (2017).
22. X. Nie et al., "Cool white polymer coatings based on glass bubbles for buildings," *Sci. Rep.* **10**(1), 6661 (2020).
23. S. Atiganyanun, "Use of hollow silica and titanium dioxide microparticles in solar reflective paints for daytime radiative cooling applications in a tropical region," *J. Photonics Energy* **11**, 022103 (2021).
24. R. Kitamura, L. Pilon, and M. Jonasz, "Optical constants of silica glass from extreme ultraviolet to far infrared at near room temperature," *Appl. Opt.* **46**(33), 8118–8133 (2007).
25. J. Kischkat et al., "Mid-infrared optical properties of thin films of aluminum oxide, titanium dioxide, silicon dioxide, aluminum nitride, and silicon nitride," *Appl. Opt.* **51**(28), 6789–6798 (2012).
26. X. Chen et al., "Systematically investigating solar absorption performance of plasmonic nanoparticles," *Energy* **216**, 119254 (2021).
27. X. Chen et al., "Modeling the solar absorption performance of Copper@Carbon core–shell nanoparticles," *J. Mater. Sci.* **56**(24), 13659–13672 (2021).
28. Z. Chen et al., "Enhanced solar thermal conversion performance of plasmonic gold dimer nanofluids," *Appl. Therm. Eng.* **178**(January), 115561 (2020).
29. X. Zhang et al., "Complex refractive indices measurements of polymers in infrared bands," *J. Quant. Spectrosc. Radiat. Transf.* **252**, 107063 (2020).
30. G. Y. Onoda and E. G. Liniger, "Random loose packings of uniform spheres and the dilatancy onset," *Phys. Rev. Lett.* **64**(22), 2727 (1990).
31. M. Chen et al., "Designing mesoporous photonic structures for high-performance passive daytime radiative cooling," *Nano Lett.* **21**(3), 1412–1418 (2021).
32. M. Chen et al., "A scalable dealloying technique to create thermally stable plasmonic nickel selective solar absorbers," *ACS Appl. Energy Mater.* **2**(9), 6551–6557 (2019).
33. M. Chen and Y. He, "Plasmonic nanostructures for broadband solar absorption based on the intrinsic absorption of metals," *Sol. Energy Mater. Sol. Cells* **188**(August), 156–163 (2018).
34. M. Chen et al., "Investigating the effective radiative cooling performance of random dielectric microsphere coatings," *Int. J. Heat Mass Transf.* **173**, 121263 (2021).

Meijie Chen is an associate professor in the School of Energy Science and Engineering at Central South University. He received his BEng, MEng, and PhD degrees from School of Energy Science and Engineering at Harbin Institute of Technology in 2014, 2016, and 2019, respectively. He was a visiting graduate student at Columbia University funded by CSC in 2018. His research interests are in the photothermal conversion, transport, storage, and applications.

Shuang Li received her bachelor's degrees from Central South University of Forestry and Technology in 2021. She is now a master student at Centre South University. Her research interests include water harvesting based on solar heating and radiative cooling.

Dan Pang received her bachelor's degrees from Centre South University in 2020. She is now a master student at Centre South University. Her research interests include radiative cooling and nanoscale thermal management.

Yanwei Zhao received her bachelor's degrees from Centre South University in 2021. She is currently pursuing her PhD at Tsinghua University. Her research interests include radiative cooling and heat & mass transfer.

Yuan Yang is associate professor in the Department of Applied Physics and Applied Mathematics, Columbia University. He received his BS degree in physics from Peking University in 2007 and his PhD in materials science and engineering from Stanford University in 2012. Then he worked as a postdoctoral researcher at MIT for three years. His research interests include electrochemical energy storage and conversion and thermal management.

Hongjie Yan is a professor in the School of Energy Science and Engineering at Central South University. He received his BEng and PhD degrees from School of Energy Science and Engineering at Central South University in 1999 and 2005, respectively. His research interests are multiphase fluid, computational fluid dynamics, and energy saving in industrial processes.